# [7] Analysis of corneal aberration of the human eye

*P.A. Khorin [1], S.N. Khonina [1, 2], A.V. Karsakov [1], S.L. Branchevsky [3]*
*[1] Samara National Research University, Samara, Russia,*
*[2] Image Processing Systems Institute of RAS,– Branch of the FSRC "Crystallography and Photonics" RAS, Samara, Russia,*
*[3] Branchevsky Eye Clinic, Samara, Russia*

Abstract

In this work, we analyze the human eye corneal aberrations based on the data obtained in the Branchevsky Eye Clinic. The analysis is performed on the basis of representation of aberrations as a superposition of Zernike functions. As the result of the analysis, we selected the Zernike basis functions which are the most characteristic for some pathologies of the eye.

**Keywords:** *corneal aberration, Zernike function, point spread function, myopia of the human eye.*
**Citation:** *Khorin PA, Khonina SN, Karsakov AV, Branchevsky SL. Analysis of corneal aberrations of the human eye. Computer Optics 2016; 40(6): 810-817.*
*DOI: 10.18287/0134-2452-2016-40-6-810-817.*

## Introduction

The human eye may be described as a lens system consisting of three principal components: cornea, pupil and crystalline lens [1]. All optical characteristics of the normal human eye are determined by means of combination of corneal aberrations and intraocular optics.

The researches [2 – 4] show that the total amount of wave aberrations in the whole eye is always smaller than aberrations of the anterior corneal surface or intraocular optics. This effect is due to the process of compensation between the cornea and the crystalline lens [5]. There are some sound arguments for compensating aberrations between the cornea and intraocular optics in the case of astigmatism, coma, and spherical aberration [6]. The overall result of the compensation process is the reduction of the value of these aberrations in the retina plane with possible improvement of the image optical quality in foveola. The value of aberrations in the cornea and crystalline lens for young people is basically higher than that one in the whole eye. This fact substantiates the earlier assumption that the crystalline lens plays important role in compensation of corneal aberrations, which results in improvement of the image quality on the retina.

In this paper, we pay special attention particularly to the anterior and posterior corneal surfaces, as the aberrations of these surfaces are very important in imaging of the human eye optical system. Besides, the correction of these particular surfaces can be easily performed in surgical procedures [7 – 9].

## *1. Description of aberrometers*

The WaveLight Oculyzer II and HD Analyzer aberrometers provided by the Branchevsky Eye Clinic were used to obtain aberrations data for the human eye optical system. The WaveLight Oculyzer II is a diagnostic device developed for characteristics determination and ophthalmic fundus examination. It is designed for visualization of the anterior surface which includes: cornea, pupil, ocular anterior chamber and the crystalline lens (Fig. 1). This device measures a corneal shape and it is specially designed for ophtalmologists. The key advantage of this research paper is that the WaveLight Oculyzer II performs the analysis of the anterior and posterior corneal surfaces and enables us to achieve the Zernike expansion of aberration functions (Fig. 2).

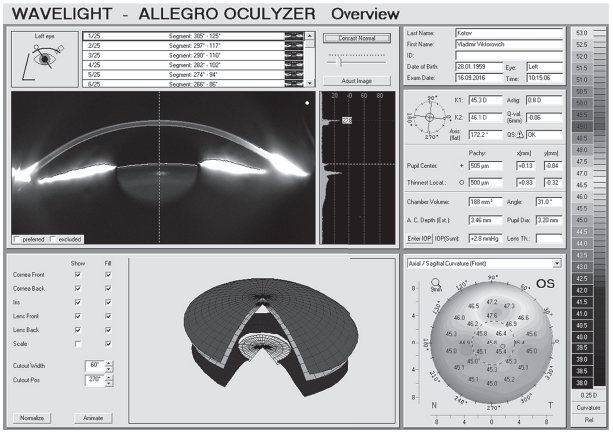


*Fig. 1. Summary report on the WaveLight Oculyzer II performance*

The wavefront expansion coefficients by the Zernike orthogonal functions [10] allow us to determine the standard mean squared deflection error of the ideal wavefront. The wavefront aberration is determined as a deviation of this wavefront from a reference surface (ideal wave). An initial surface is usually defined as the wavefront curvature surface which derives from a Gaussian image point (where the light would be focused if the eye was ideal).

The image quality evaluation consists in watching test objects, measuring photometric characteristics, and determining the point spread function (PSF) and the line spread function. In practice, these particular characteristics demonstrate quantitatively the image quality of the optical system. The quality evaluation methods for this kind of images have one great advantage – they consider every single causes involved in real optical imaging.

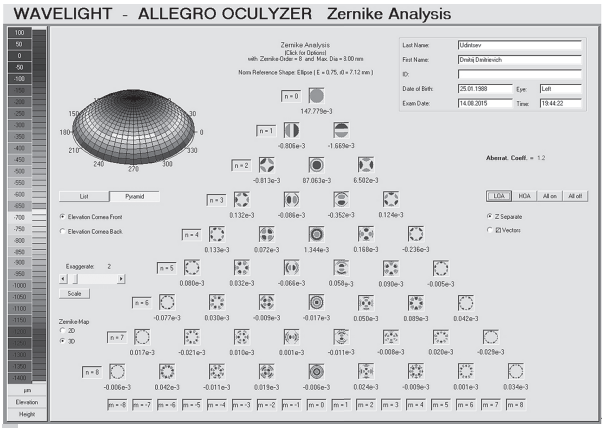


*Fig. 2. A Zernike pyramid with the weighing factors for the anterior corneal surface*

The point spread function found experimentally characterizes the system quality. It allows us to consider all of the features of the system-generated wave surface, including a microrelief pattern of optical surfaces, such as the posterior and anterior corneal surfaces [11].

The data collected by the HD Analyzer recording device are also used in this paper. It is a tool based on the light double pass technique, which provides objective clinical assessment of the quality of the eye optics.

A light source is projected on the retina. For this purpose, the light goes twice through the ocular medium: before and after retina reflection. The HD Analyzer analyzes the size and shape of the reflected light spot.

The optical diagram of the device is shown in Fig. 3. The light source is a laser diode 780 nm in wavelength. The light beam is filtered and collimated by means of L1. After the beam is reflected and passed through the beam splitter BS, it goes through the achromatic lenses L2 and L3 and corrector FC (with two neighboring mirrors) with a varying focus [12].

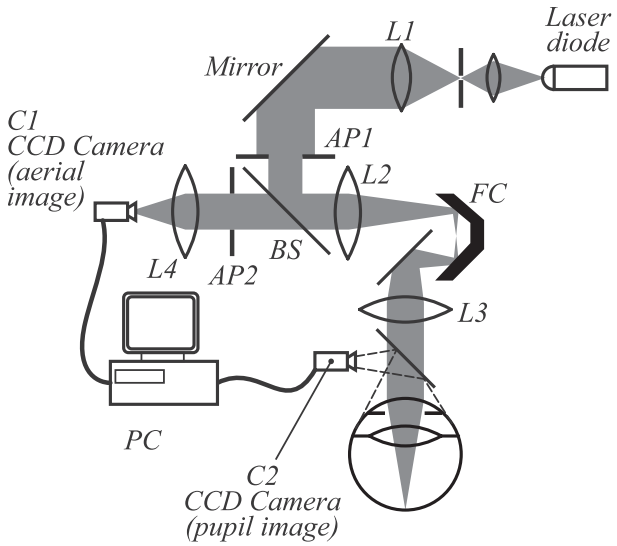


*Fig. 3. Typical diagram of the HD Analyzer*

Ocular spherical refraction is corrected by changing optical distances between L2 and L3.

The HD Analyzer images contain information on the quality of the ocular optical system, including the high order aberrations, however, in this case only PSF is visualized (Fig. 4), whereas the contribution of separate aberrations is not detailed. The high order aberrations are important for refractive surgery.

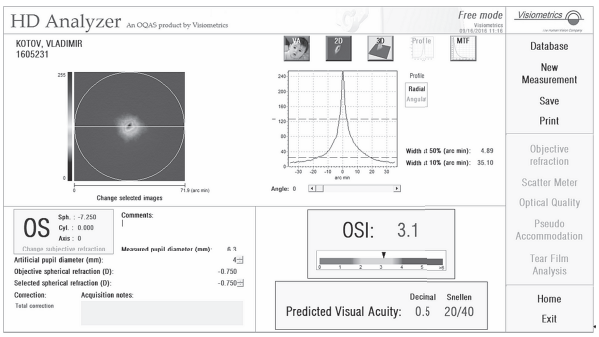


*Fig. 4. Summary report on the HD Analyzer performance*

## *2. Typical aberrations*

Each Zernike basis function is related to a special type of optical errors or wavefront deviations (Table 1). The deviations may be described as a combi-

nation of basic aberrations, which are better known for ophthalmology professionals.

*Table1. Relationship of the Zernike functions and types of aberrations*

| *N* | *n* | *m* | Trigonometric representation | Types of aberrations |
|---|---|---|---|---|
| 1 | 0 | 0 | 1 | Constant |
| 2 | 1 | −1 | $2r\sin(\theta)$ | Tilt |
| 3 | 1 | 1 | $2r\cos(\theta)$ | Tilt |
| 4 | 2 | −2 | $\sqrt{6}r^2\sin(2\theta)$ | Astigmatism |
| 5 | 2 | 0 | $\sqrt{3}(2r^2-1)$ | Defocus |
| 6 | 2 | 2 | $\sqrt{6}r^2\cos(2\theta)$ | Astigmatism |
| 7 | 3 | −3 | $2\sqrt{2}r^3\sin(3\theta)$ | Zero curvature Coma (Trefoil) |
| 8 | 3 | −1 | $2\sqrt{2}(3r^3-2r)\sin(\theta)$ | Pure coma |
| 9 | 3 | 1 | $2\sqrt{2}(3r^3-2r)\cos(\theta)$ | Pure coma |
| 10 | 3 | 3 | $2\sqrt{2}r^3\cos(3\theta)$ | Zero curvature Coma (Trefoil) |
| 11 | 4 | −4 | $\sqrt{10}r^4\sin(4\theta)$ | Quadrofoil |
| 12 | 4 | −2 | $\sqrt{10}(4r^4-3r^2)\sin(2\theta)$ | 2th order Astigmatism |
| 13 | 4 | 0 | $\sqrt{5}(6r^4-6r^2+1)$ | Spherical |
| 14 | 4 | 2 | $\sqrt{10}(4r^4-3r^2)\cos(2\theta)$ | 2th order Astigmatism |
| 15 | 4 | 4 | $\sqrt{10}r^4\cos(4\theta)$ | Quadrofoil |

The Zernike functions are considered in this paper as follows:

$$Z_{nm}(r,\varphi)=\sqrt{\frac{n+1}{\pi r_0^2}}R_n^m(r)\begin{Bmatrix}\cos(m\varphi)\\ \sin(m\varphi)\end{Bmatrix}, \quad (1)$$

where $R_n^m(r)$ are the Zernike radial polynomials.
The numbering sequence and normalization of the Zernike functions may be performed in different ways; therefore, in each individual case it must be specially stated.
The wavefront aberrations detected in optical systems are usually described in terms of the Zernike basis functions as follows [10]:

$$W(r,\varphi)=\exp\left[i\psi(r,\varphi)\right], \quad (2)$$

$$\psi(r,\varphi)=\sum_{n=0}^{N}\sum_{m=-n}^{n}c_{nm}Z_{nm}(r,\varphi). \quad (3)$$

For easy visual representation, Figure 5 shows a "Zernike pyramid" consisting of several first Zernike functions. The radial numbers vary vertically from $n=0$ to 4, whereas the azimuth numbers vary horizontally from $m=-n$ to $m=n$.

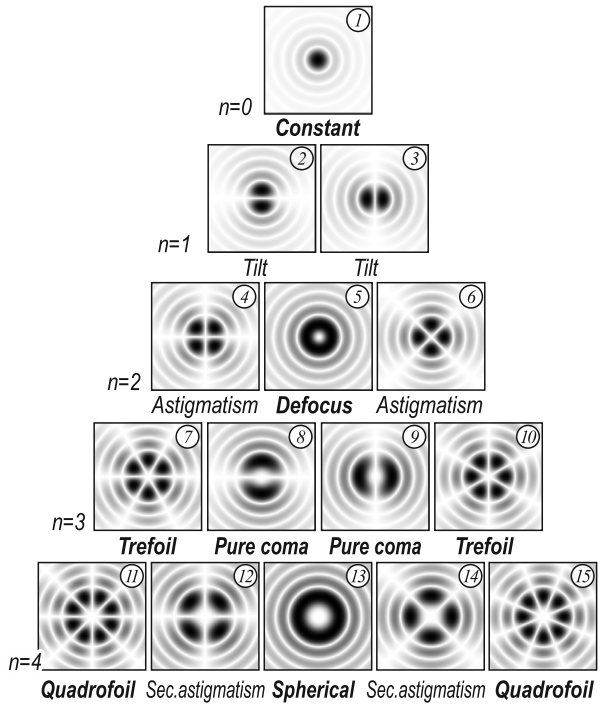


*Fig. 5. Patterns of several Zernike functions*

To construct PSF patterns in the presence of typical aberrations, we used the simplest optical system of the Fourier correlator in Zemax software[13].
Two equal lenses made of BK8 glass are used in the optical diagram given in Fig. 6.

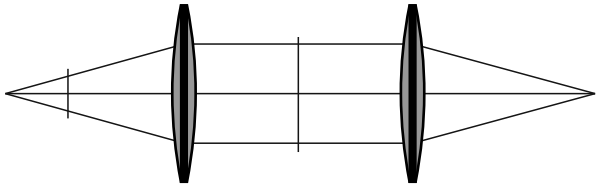

*Fig. 6. Optical diagram of the Fourier correlator*

The system aperture diaphragm 3 mm in radius is located in the center of the diagram. In simulation, the wavelength was 780 nm. When setting the radius of normalization by Zernike polynomials, we used not the lens radius, but the exit pupil radius calculated in Zemax, which was 8.37 mm.

The third-order coma (Fig. 7) was added to the first surface of the second lens that corresponds to the Zernike function (3,1) (the coefficient was selected as being equal to 1).

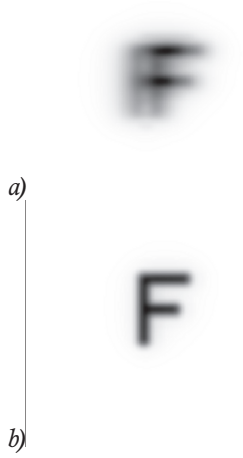

*a)*

*b)*

*c)*

*d)*

*Fig. 7. PSF in the absence of aberration (a), coma (b) and relevant test images (c, d)*

We will make use of the following algorithm to simulate a similar system. We will construct a wavefront as a superposition of Zernike polynomials using formulas (1) – (3). Then we will calculate PSF as the Fourier transform of the pupil function (2) in the coherent case. For easy visual representation, Figure 8 shows a "PSF pyramid" corresponding to the Zernike pyramid.

The coherent PSF (Fig. 8) obtained by means of the Fourier transform is close to aberration curves (Fig. 7) obtained by modeling in Zemax.

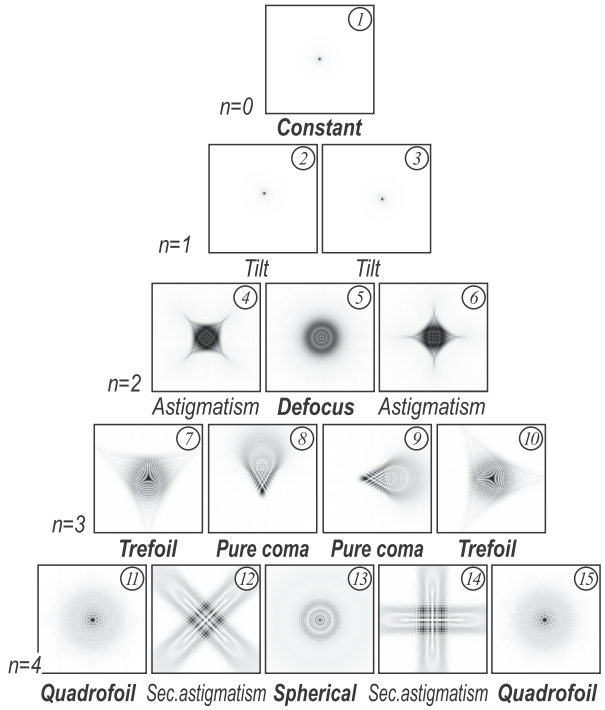


*Fig. 8. Patterns of PSFs corresponding to typical aberrations*

Note that in addition to the numbering and normalization, the Zernike functions may differ in the angular dependence. In particular, for the analysis of the wavefront we considered both exponential and trigonometric angular dependence using multichannel diffractive optical elements [14 – 17]. Moreover, in the first case, there is the rotation invariance of the Zernike basis [18]. In the second case, when rotating the picture (Fig. 9), the coefficients for the Zernike basis functions will be changed.

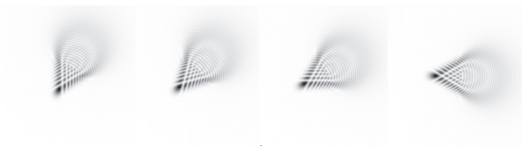

*Fig. 9. Rotating PSF of the Zernike function n = 3, m = 1, $\phi_0 = \{0, \pi/6, \pi/4, \pi/3, \pi/2, \pi, 3\pi/2, 2\pi\}$*

The possibility of calculating the field angle rotation by $\phi_0$ is provided by the following superposition:

$$\psi(r,\varphi) = R_{nm}(r)\left[a\sin(m\varphi) + b\cos(m\varphi)\right], \qquad (4)$$

where $a = \sin(|m|\varphi_0)$, $b = \cos(|m|\varphi_0)$, $\phi_0 \in [0; 2\pi]$.

### 3. Basic aberrations of the ocular optical system

In our research, we used the data obtained in the Branchevsky Eye Clinic in the fall of 2016 both for conventionally healthy people (without evident pathologies in the pupil and crystalline lens) and for patients with certain pathologies, particularly, with low and moderate myopia.

The cornea (including the tear film) is a dominant structure of the optical power of the human eye (on average, about 70%). It is accordingly the main source of aberrations in the human eye. The anterior corneal surface has an elongated profile; so its center is sharper than its periphery. This form helps us to decrease the value of spherical aberrations throughout the whole eye. However, corneal shapes differ significantly for different people, and this leads to astigmatism and high-order asymmetric aberrations (e.g., coma).

A corneal reference model can be sphere- or ellipsoid-shaped with average eccentricity equaled to the measured one or ellipsoid-shaped with eccentricity of 0.75. The reference model is always axially symmetric, and its shape influences only the coefficients of the axially symmetric Zernike functions (1) with numbers $(n, 0)$.

The central radius of the reference model is always taken up as the central average measurement radius. In the absence of the reference model, the largest contribution to the shape of the cornea is made by a component corresponding to the Zernike function (2, 0) (a paraboloid), since this component bears the greatest similarity to the corneal shape.

Figure 10 shows the optical diagram that enables us to implement the simplest eye model in Zemax [18]. The wavelength in simulation was 780 nm (the same wavelength is used by the HD Analyzer).

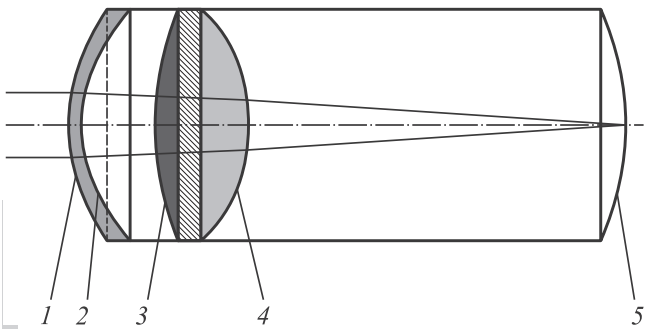


*Fig. 10. Layout diagram of basic refracting surfaces of the human eye: 1 – the anterior corneal surface, 2 – the posterior corneal surface, 3 – the anterior surface of the crystalline lens, 4 – the posterior surface of the crystalline lens, 5 – the retina*

Various aberrations were subsequently added to the corneal surface. Figure 11 represents the optical system operating with coma added to the anterior corneal surface corresponding to the Zernike function (3, 1) with the factor of 1.

When setting the radius of normalization by the Zernike polynomials, we used not the lens radius, but the exit pupil radius calculated in Zemax that was 100 mm.

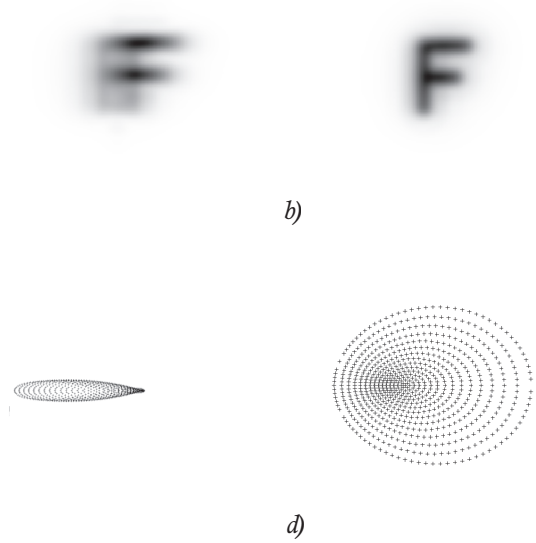


*Fig. 11. PSF in the absence of aberration (a), in the presence of coma (b) and relevant test images (c, d)*

The simplest statistical analysis was performed within the framework of the present research based on sampling 150 measurements. The corneal surfaces (anterior and posterior surfaces) were independently examined for various patient volunteers (with healthy crystalline lenses). The patients were grouped according to their age (20-29 and 30-39 years) and diagnoses (low and moderate myopia).

The WaveLight Oculyzer II aberrometer enables us to obtain separately the Zernike coefficients for the anterior and posterior corneal surfaces. The average values thereof are given in Figures 12–15. For visual clarity of the Zernike coefficients, we excluded from consideration (set to zero) the coefficients, corresponding to the functions with numbers $(n, 0)$, $n = 0, 2, 4$. Values of the weighting coefficients of these functions are substantially higher than all the others, but they contain no information on any deviations.

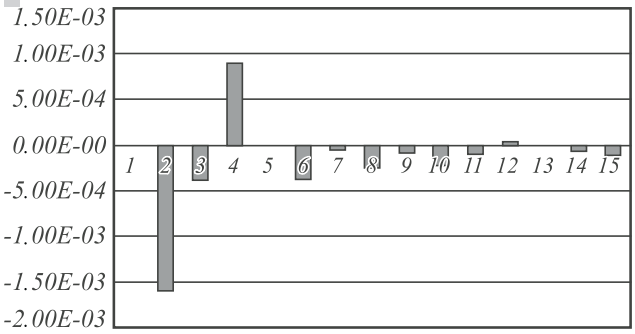


*Fig. 12. Values of the weighting cofficients of the Zernike polynomials for the anterior corneal surface in healthy people*

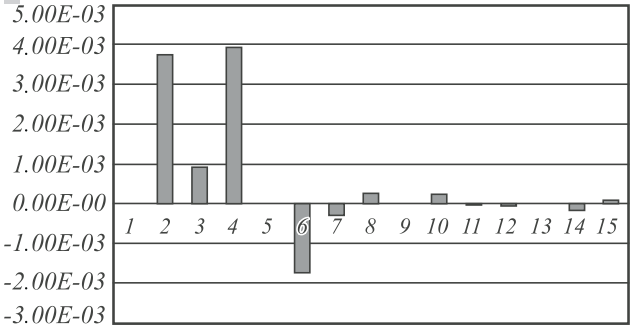


*Fig. 13. Values of the weighting cofficients of the Zernike polynomials for the posterior corneal surface in healthy people*

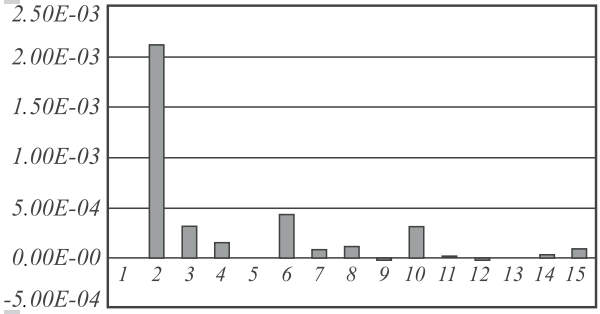


*Fig. 14. Values of the weighting cofficients of the Zernike polynomials for the anterior corneal surface in people with low myopia*

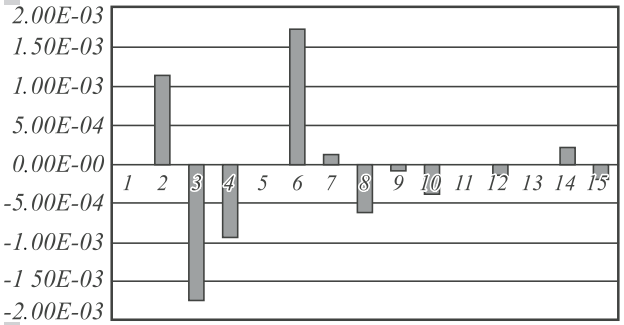


*Fig. 15. Values of the weighting cofficients of the Zernike polynomials for the posterior corneal surface in people with low myopia*

Figure 16 shows distributions corresponding to the average aberrations of the anterior corneal surface at a diagnosis of low myopia (SE from 1 to 5 diopters) and also an appropriate PSF. The same distributions for the posterior corneal surface are shown in Fig. 17. To assess the influence of corneal aberrations as a whole, the wavefront aberrations were added up; the corresponding result is shown in Fig. 18.

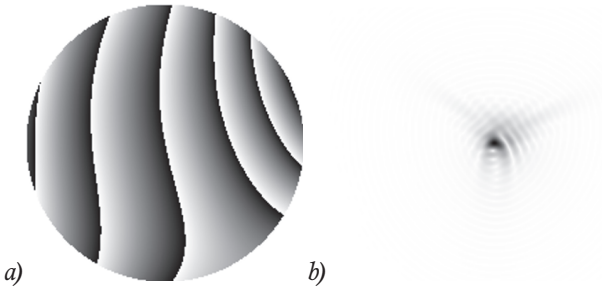


*Fig. 16. The average aberrations of the angterior corneal surface for diagnosis of low myopia: the wavefront (a) and PSF (b)*

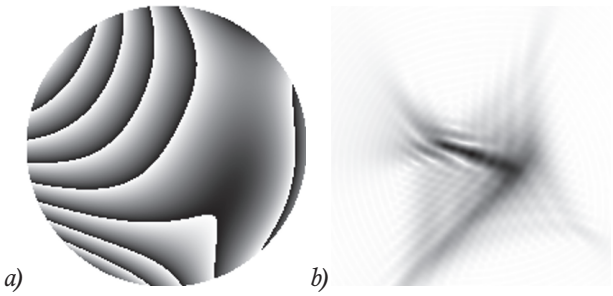


*Fig. 17. The average aberrations of the posterior corneal surface for diagnosis of low myopia: the wavefront (a)and PSF(b)*

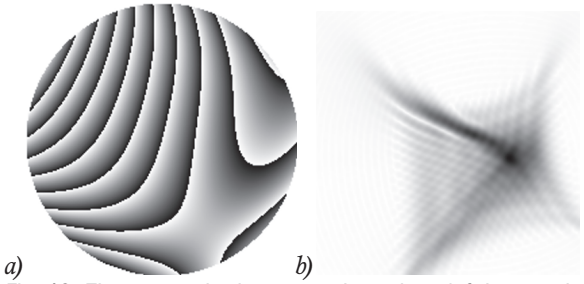


*Fig. 18. The summarized average aberrations (of the anterior and posterior corneal surfaces) for diagnosis of low myopia: the wavefront (a) and PSF (b)*

The result for diagnosis of moderate myopia was obtained in a similar way (SE from 5 to 10 diopters, Fig. 19).

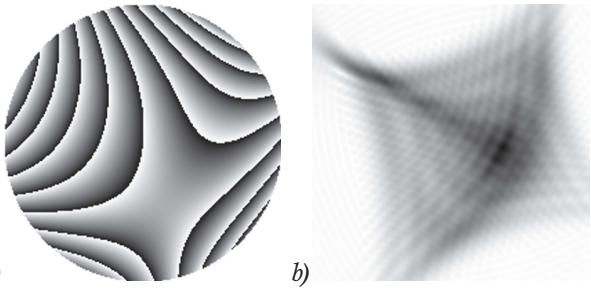

a) b)

*Fig. 19. The summarized average aberrations (of the anterior and posterior corneal surfaces) for diagnosis of moderate myopia: the wavefront (a) and PSF (b)*

Based on the statistical analysis findings, it was found that the most evident Zernike coefficients corresponded to a proper diagnosis that is shown in Table 2.
It should be noted that a slight increase of the average spherical aberration is generally observed with aging. A moderate increase in spherical aberration is associated with changing corneal asphericity over time [19]. The anterior corneal surface has a tendency toward less elongating with aging, whereas no significant age-related changes of the posterior corneal surface can be observed.

*Table 2. Summary table for the anterior and posterior corneal surfaces: the relation of diagnoses and the Zernike polynomials with the largest weighting coefficients (the notations correspond to Fig. 5, 8)*

| **Anterior** | |
|---|---|
| Low myopia | Moderate myopia |
| (1,−1); (2,2) | (1,−1); (1,1); (2,2); (3,3) |
| **Posterior** | |
| Low myopia | Moderate myopia |
| (2,2); (1, 1); (1,−1); (2,−2) | (2,2); (2,−2); (3,−1) |

## Conclusion

Within the framework of this research, we analyzed corneal aberrations of the human eye based on the data obtained in the Branchevsky Eye Clinic in the fall of 2016. The analysis was performed on the basis of representation of aberrations in the form of a superposition of the Zernike functions. As the result of the analysis (where we excluded from consideration the coefficients corresponding to the functions with numbers $(n,0)$, $n=0,2,4)$, we selected the Zernike basis functions which are the most characteristic for some pathologies of the human eye.
In particular, while selecting patients with low myopia, some slopes were detected both on the anterior and posterior corneal surfaces, whereas astigmatism was captured much more (especially on the posterior corneal surface). The influence of the third-order coma is now more important than ever for moderate myopia, as detected in the sampling analysis. In addition, aberrations typical of low myopia continue to remain too.

## Acknowledgements

This work was financially supported by the Rusian Foundation for Basic Research (grant 15-29-03823).

## References

**1.** Lombardo M, Lombardo G. Wave aberration of human eyes and new descriptors of image optical quality and visual performance. Journal of Cataract & Refractive Surgery 2010; 36(2): 313-331. DOI: 10.1016/j.jcrs.2009.09.026.

**2.** Artal P, Guirao A, Berrio E, Williams DR. Compensation of corneal aberrations by the internal optics in the human eye. J Vis 2001; 1(1): 1-8. DOI: 10.1167/1.1.1.

**3.** Artal P, Berrio E, Guirao A, Piers P. Contribution of the cornea and internal surfaces to the change of ocular aberrations with age. Journal of the Optical Society of America A 2002; 19(1): 137-143. DOI: 10.1364/JOSAA.19.000137.

**4.** He JC, Gwiazda J, Thorn F, Held R. Wave-front aberrations in the anterior corneal surface and the whole eye. Journal of the Optical Society of America A 2003; 20(7): 1155-1163. DOI: 10.1364/JOSAA.20.001155.

**5.** Mrochen M, Jankov M, Bueeler M, Seiler T. Correlation between corneal and total wavefront aberrations in myopic eyes. Journal of Refractive Surgery 2003; 19(2): 104-112. DOI: 10.3928/1081-597X-20030301-04.

**6.** Kelly JE, Mihashi T, Howland HC. Compensation of corneal horizontal/vertical astigmatism, lateral coma, and spherical aberration by internal optics of the eye. Journal of Vision 2004; 4(4): 262-271. DOI: 10.1167/4.4.2.

**7.** Farah SG, Azar DT, Gurdal C, Wong J. Laser in situ keratomileusis: literature review of a developing technique. Journal of Cataract Refractive Surgery 1998; 24(7): 989-1006.

**8.** Roberts C. Biomechanics of the Cornea and Wavefront-Guided Laser Refractive Surgery. Journal of Refractive Surgery. 2002; 18(5): S589-S592.

**9.** O'Keefe M, O'Keeffe N, Corneal Surgical Approach in the Treatment of Presbyopia. Journal of Clinical & Experimental Ophthalmology 2016; 7(1): 512. DOI: 10.4172/2155-9570.1000512.

**10.** Born M, Wolf E. Principles of Optics: Electromagnetic Theory of Propagation, Interference and Diffraction of Light. 7th ed. Cambridge: Cambridge University Press; 1999.

**11.** Kirilovskiy VK. Optical measures. Part II. The theory of sensitivity optical measuring levelling. The role of the optical image. Schoolbook [In Russian]. Saint-Petersburg: "SPb. GITMO (TU)" Publisher; 2003.

**12.** HD Analyzer® User's Manual. Visiometrics; 2012.

**13.** Zemax® User's Guide. Zemax Development Corporation; 2005.

**14.** Khonina SN, Kotlyar VV, Wang Ya. Diffractive optical element matched with Zernike basis. Pattern Recognition and Image Analysis 2001; 11(2): 442-445.

**15.** Khonina SN, Kotlyar VV, Kirsh DV. Zernike phase spatial filter for measuring the aberrations of the optical structures of the eye. Journal of Biomedical Photonics & Engineering 2015; 1(2): 146-153.

**16.** Kirilenko MS, Khorin PA, Porfirev AP. Wavefront analysis based on Zernike polynomials. CEUR Workshop Proceedings 2016; 1638: 66-75. DOI: 10.18287/1613-0073-2016-1638-66-75.

**17.** Porfirev AP, Khonina SN. Experimental investigation of multi-order diffractive optical elements matched with two types of Zernike functions. Proc SPIE 2016; 9807: 98070E. DOI: 10.1117/12.2231378.

**18.** Tocci M. How to Model the Human Eye in Zemax. Source: http://www.zemax.com/os/resources/learn/knowledgebase/how-to-model-the-human-eye-in-zemax.

**19.** [19] Guirao A, Redondo M, Artal P. Optical aberrations of the human cornea as a function of age. J Opt Soc Am A 2000; 17(10): 1697-1702.